PLANT SCIENCES

BLADE-ON-PETIOLE interacts with CYCLOIDEA to fine-tune *CYCLOIDEA*-mediated flower symmetry in monkeyflowers (*Mimulus*)

Yuan Gao¹†, Jingjian Li²†, Jiayue He¹†, Yaqi Yu¹, Zexin Qian¹, Zhiqiang Geng¹, Liuhui Yang¹, Yumin Zhang¹, Yujie Ke¹, Qiaoshan Lin³‡, Jing Wang¹, Sumei Chen^{1,4}, Fadi Chen^{1,4}, Yao-Wu Yuan^{3,5}, Baoqing Ding^{1,3,4}*

Morphological novelties, or key innovations, are instrumental to the diversification of the organisms. In plants, one such innovation is the evolution of zygomorphic flowers, which is thought to promote outcrossing and increase flower morphological diversity. We isolated three allelic mutants from two *Mimulus* species displaying altered floral symmetry and identified the causal gene as the ortholog of *Arabidopsis BLADE-ON-PETIOLE*. We found that MIBOP and MICYC2A physically interact and this BOP-CYC interaction module is highly conserved across the angiosperms. Furthermore, MIBOP self-ubiquitinates and suppresses *MICYC2A* self-activation. MICYC2A, in turn, impedes MIBOP ubiquitination. Thus, this molecular tug-of-war between MIBOP and MICYC2A fine-tunes the expression of *MICYC2A*, contributing to the formation of bilateral symmetry in flowers, a key trait in angiosperm evolution.

Copyright © 2024 me
Authors, some rights
reserved; exclusive
licensee American
Association for the
Advancement of
Science. No claim to
original U.S.
Government Works.
Distributed under a
Creative Commons
Attribution
NonCommercial
License 4.0 (CC BY-NC).

INTRODUCTION

Morphological novelties, or key innovations, are instrumental to the diversification of the organisms (1, 2). In plants, one such innovation is the evolution of zygomorphic flowers, which differentiate along the dorsiventral axis and are thought to enhance diverse pollinator exploitation for promoting outcrossing (3) and increasing flower morphological diversity (2). Floral zygomorphy has evolved multiple times independently in many angiosperm lineages from their actinomorphic ancestors (4-6). Because of its prevalence, essential ecological functions, and evolutionary implications, the molecular mechanisms underpinning floral zygomorphy have been extensively investigated in many plant lineages. The common garden snapdragon (Antirrhinum) is one of the best investigated systems: Two functionally redundant and dorsally expressed genes, CYCLOIDEA (CYC) and DICHOTOMA (DICH) (7, 8), activate RA-DIALIS (RAD) (9) in the dorsal petals. RAD, in turn, competes with two DIV-RAD interacting factors (10) to bind with DIVARICATA (DIV) (11, 12), establishing zygomorphy. This model has been widely adopted to explain the alteration of floral symmetry in many plant lineages.

Central to the model is the spatially restricted expression pattern of *CYC*, as expanding its expression leads to dorsalized actinomorphy (7). This spatial expansion of the *CYC*-like genes has been documented in various taxa, converting flowers from zygomorphy to actinomorphy (13–22). However, the evolutionary shifts from zygomorphy

¹State Key Laboratory of Crop Genetics & Germplasm Enhancement and Utilization; Key Laboratory of Landscaping, Ministry of Agriculture and Rural Affairs; Key Laboratory of State Forestry and Grassland Administration on Biology of Ornamental Plants in East China; College of Horticulture, Nanjing Agricultural University, Nanjing 210095, P. R. China. ²College of Pharmacy, Guillin Medical University, Guilin 541199, P. R. China. ³Department of Ecology and Evolutionary Biology, University of Connecticut, Storrs, CT 06269, USA. ⁴Zhongshan Biological Breeding Laboratory, No.50 Zhongling Street, Nanjing 210014, P. R. China. ⁵Institute for Systems Genomics, University of Connecticut, Storrs, CT 06269, USA.

*Corresponding author. Email: ding.baoqing@njau.edu.cn

†These authors contributed equally to this work.

‡Present address: Center for Research Informatics, University of Chicago, IL 60637, USA.

to actinomorphy have often involved a reduced number of petals, unlike the increased number observed in the *Antirrhinum cyc* mutant (11), implying additional underlying mechanisms beyond simple changes in the *CYC* expression domain (4, 23, 24). Despite that the association between the alteration of flower symmetry and the changes in *CYC* expression pattern has long been established, how the expression of *CYC* is regulated and whether additional genetic factors are involved remain largely unknown.

BLADE-ON-PETIOLE (BOP) encodes an ancient and conserved family of plant-specific transcriptional coactivators that regulates a plethora of plant developmental processes (25). Though early studies were primarily focused on its role in leaf development (26, 27), emerging studies drawing from monocots and eudicots indicate that it is also essential in regulating inflorescence (28, 29) and flower development (30–33). Intriguingly, Arabidopsis, Medicago, and Pisum bop mutants exhibited a change in flower symmetry (30, 32, 34). However, whether these changes involve the alteration of CYC expression remains elusive.

In this study, we used a chemical mutagenesis approach to screen for mutants with altered flower symmetry in the monkeyflower species Mimulus lewisii and Mimulus verbenaceus. We isolated three allelic mutants displaying altered floral symmetry, with notably upregulated expression of CYC. Genomic and Sanger sequencing revealed three independent mutations in the ortholog of Arabidopsis BLADE-ON-PETIOLE (BOP) in these mutants. Functional analyses further validated that BOP is the causal gene underlying the mutants. The overlapping of the spatiotemporal expression patterns of MlBOP and MlCYC2A, as revealed by in situ hybridization analysis, suggests that MlBOP might directly regulate the expression of Ml-CYC2A. Unexpectedly, we found that MIBOP and MICYC2A physically interact, and this BOP-CYC interaction module is highly conserved across the angiosperms. Furthermore, we revealed that MIBOP functions as an E3 ligase adaptor to self-ubiquitinate but does not ubiquitinate its interacting partner MlCYC2A. Instead, MIBOP suppresses the self-activation of MICYC2A. MICYC2A, on the other hand, impedes the ubiquitination of MIBOP. Thus, this

molecular tug-of-war between MIBOP and MICYC2A fine-tunes the expression of *MICYC2A*, contributing to the formation of bilaterally symmetrical flowers in *Mimulus*.

RESULTS

Phenotypic characterization of the floral symmetry mutants in *Mimulus*

The corolla of the wild-type *M. lewisii* (LF10) is composed of three types of petals arranged asymmetrically along the adaxial-abaxial axis: two larger dorsal petals on the adaxial side, two lateral petals, and one ventral petal on the abaxial side. Within the ventral petal, two yellow ridges were decorated with nectar guide trichomes and anthocyanin spots (Fig. 1A). Despite the well-established relationship between flower symmetry and the spatiotemporal expression pattern of *CYC* in many flowering plants (35), how the expression pattern of *CYC* is regulated remains elusive. To address this, we conducted a forward genetics screen for ethyl methanesulfonate

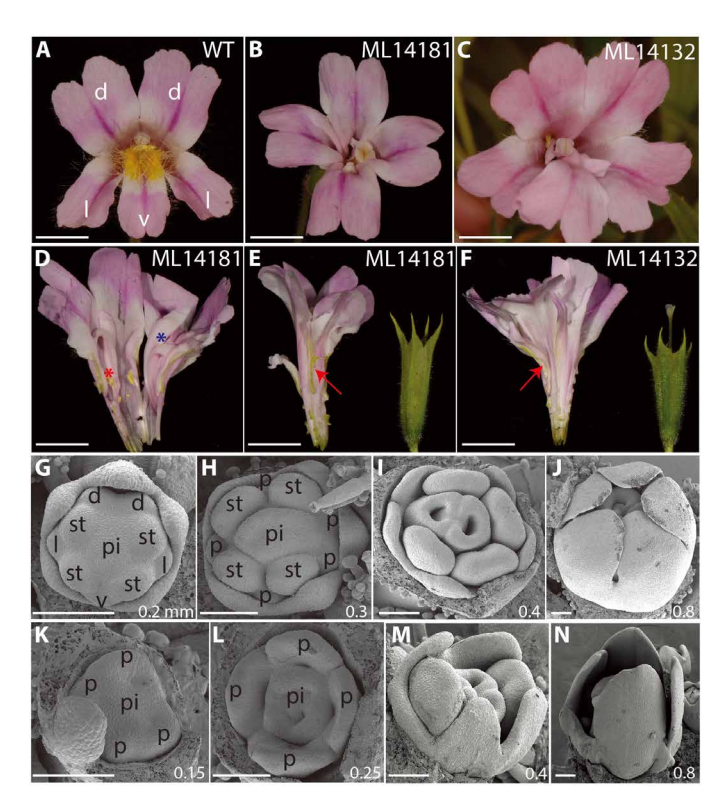


Fig. 1. Phenotypic characterization of the two floral symmetry mutants in *Mimulus lewisii*. (A to **C**) Face view of the wild-type (WT) *M. lewisii* (inbred line LF10), ML14181, and ML14132 mutant corolla. d, dorsal; l, lateral; v, ventral. Scale bars, 10 mm. (**D**) Homeotic transitions from stamens to petaloid organs in ML14181. Red asterisk labels a petaloid organ, and blue asterisk labels an extra petaloid organ. Scale bar, 10 mm. (**E** and **F**) Side view of the ML14181 and ML14132 corolla and calyx. Arrows point to the extra tissues developed between the calyx and corolla whorl and the green tissues developed in the interprimordial region. Scale bars, 10 mm. (**G** to **J**) SEM on WT flower buds at different developmental stages. p, petal; st, stamen; pi, pistil. The developmental stages are marked on the bottom right of each image by the diameter (millimeters) of the corolla. Scale bars, 100 μm. Reproduced with permission (*68*). Copyright 2020, Oxford University Press. (**K** to **N**) SEM on the ML14181 flower buds at different developmental stages. Scale bars, 100 μm.

(EMS)-induced mutants displaying altered flower symmetry in the LF10 background. We isolated two morphologically similar mutants (ML14181 and ML14132). Both mutants exhibited a transition of flower symmetry from zygomorphy to actinomorphy, as the size of their lateral and ventral petals in both mutants was similar to the two dorsal petals (Fig. 1, B and C). Notably, unlike the ML14132 mutant, the ML14181 mutant flowers had four petals instead of five, along with misregulations of floral organ identity, such as the outgrowth of extra petaloid floral organs between the sepal and petal whorl, and the homeotic transformations in the stamen whorl (Fig. 1, D to F). Furthermore, the disruption of intraorgan boundaries was evident with the development of green tissues between the petals in both mutants (Fig. 1, E and F), which was likely due to incomplete separation of the sepal and petal whorl. The number of extra tissues also varied among flowers (table S1). To ascertain whether the two phenotypically similar mutants were caused by the same gene, we conducted a complementation cross and found that the resulting F₁ progeny failed to rescue the mutant phenotypes, indicating allelism. Thus, we focused on the more severe ML14181 mutant and characterized its floral morphology using scanning electron microscopy (SEM). Early flower development in the ML14181 mutant (Fig. 1, K to N) showed clear differences compared to the wild type (Fig. 1, G to J), including the presence of only four petal primordia and delayed or aborted stamen initiation (Fig. 1, K to M, and fig. S1).

In addition, we identified a mutant, NJ01339, in M. verbenaceus (MvBL), displaying similar floral phenotypes to the two mutants in LF10 (table S1). The wild-type M. verbenaceus corolla exhibited a similar symmetry plan to M. lewisii (Fig. 2A), with the two reflexed dorsal petals on the adaxial side, two lateral petals, and one ventral petal on the abaxial side, which is decorated with nectar guide trichomes but no anthocyanin spots. The NJ01339 mutant flowers had four to five nearly identical petals (Fig. 2B), with the near absence of nectar guide trichomes in the ventral petal, indicating that the ventral petal identity has been converted. To investigate whether the mutations in the three mutants from the two species were allelic, we performed interspecies complementation crosses. The F₁ hybrids derived from the mutants exhibited nearly radial symmetrical flowers with petaloid organs developed in the stamen whorl (Fig. 2, C to E). The F₁ from the cross between ML14181 and NJ01339 (Fig. 2D) had more petaloid organs in the stamen whorl compared to the F₁ from the cross between ML14132 and NJ01339 (Fig. 2E), suggesting that these three alleles were likely hypomorphic. Together, the results of the complementation crosses indicate that the mutants uncovered from M. verbenaceus, along with ML14181 and ML14132 mutants, likely represent three alleles of the same gene.

Shift from zygomorphy to actinomorphy in the mutants is correlated with the ectopic expression of CYCLOIDEA in Mimulus

Flower dorsalization is often associated with changes in the spatiotemporal expression of CYC-like genes (3). Similar to many species in Lamiales, two functionally redundant CYC-like genes, MlCYC2A and MlCYC2B (fig. S2A), were previously identified (19, 36). Both genes were expressed at relatively low levels in LF10 flower buds across different developmental stages (fig. S2B). Notably, in the ML14181 background, MlCYC2A and MlCYC2B were up-regulated by nearly eight- and fivefold, respectively, as revealed by quantitative reverse transcription polymerase chain reaction (RT-qPCR) assay

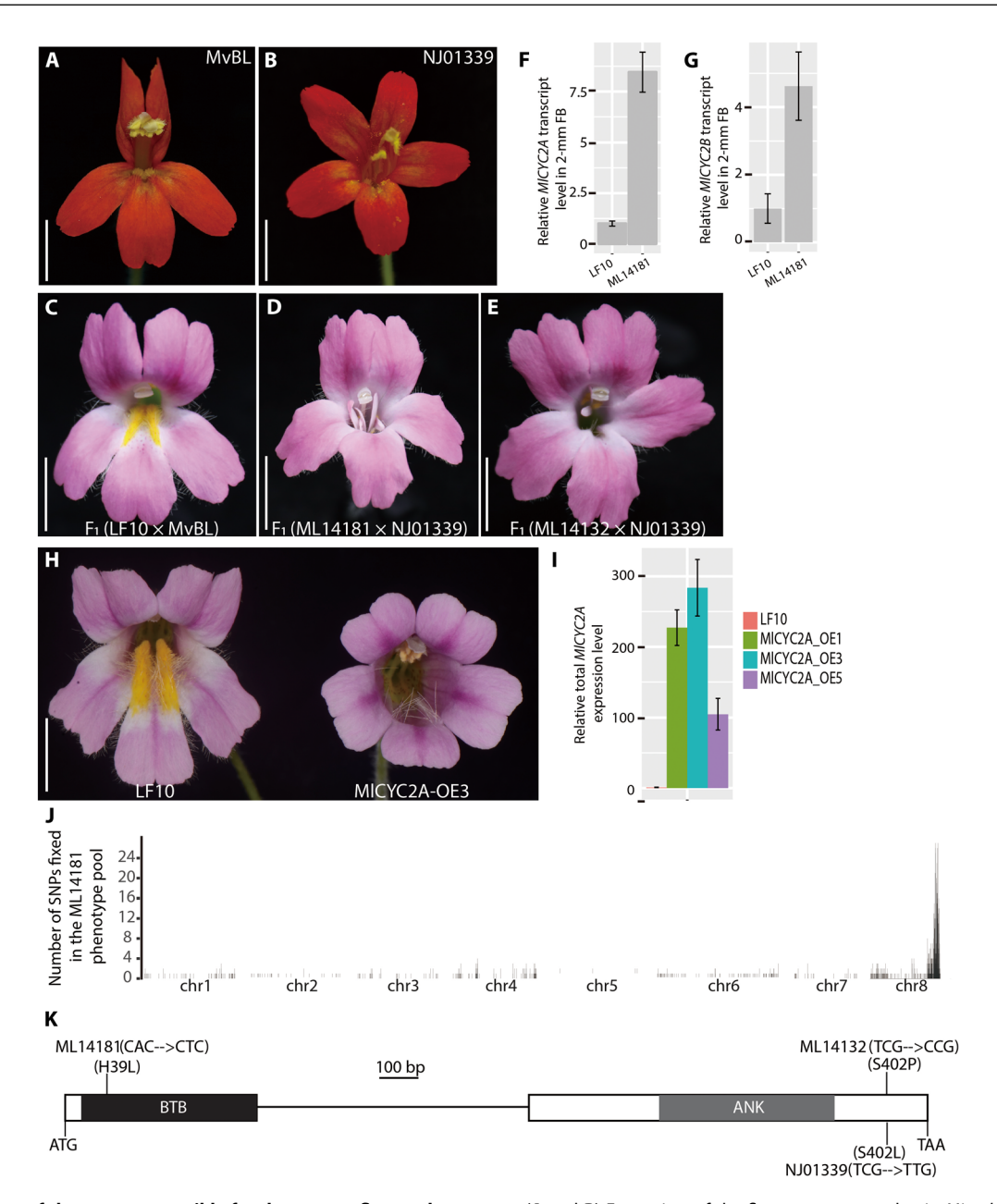


Fig. 2. Identification of the gene responsible for the mutant flower phenotypes. (A and B) Front view of the flower symmetry plan in *Mimulus verbenaceus* and NJ01339, respectively. Scale bars, 10 mm. (C) Face view of the flower phenotype of the F₁ derived from the interspecies hybridization between the WT *M. lewisii* and *M. verbenaceus*. Scale bar, 10 mm. (D and E) Flower phenotypes of the individuals derived from the interspecies complementation crosses between *M. lewisii* and *M. verbenaceus* mutants. Scale bars, 10 mm. (F and G) Quantitative measurement of *MICYC2A* and *MICYC2B* expression in WT and ML14181. *MIUBC* was used as the reference gene. Error bars represent 1 SD from three biological replicates. (H) Comparison of flower symmetry phenotype between WT and 35S: *MICYC2A* in the LF10 background. Scale bar, 10 mm. (I) Total *MICYC2A* expression level in the WT and three representative 35S: *MICYC2A* transgenic lines. *MIUBC* was used as the reference gene. Error bars represent 1 SD from three biological replicates. (J) Genome scan for regions that are enriched in homozygous SNPs reveals a sharp peak. Each pseudoscaffold of the *M. lewisii* SL 9 (the mapping line) genome was binned into 20-kb intervals, and the number of homozygous SNPs in each 20-kb interval was plotted in a bar graph. (K) The exon-intron structure of *Mimulus BOP*. A nonsynonymous substitution (A to T) causes the amino acid replacement from histidine to leucine at position 39 (H39L) for ML14181 and a nonsynonymous substitution (T to C) causes the amino acid replacement from serine to proline (S402P) for ML14132, and a nonsynonymous substitution (C to T) causes the amino acid replacement from serine to proline (S402P) for ML14132, and a nonsynonymous substitution (T to C) causes the amino acid replacement from serine to proline (S402P) for ML14132, and a nonsynonymous substitution (T to C) causes the amino acid replacement from serine to proline (S402P) for ML14132, and a nonsynonymous substitution (T to C) causes the amino acid

(Fig. 2, F and G), suggesting that the alteration of the *CYC* gene expression patterns may be linked to the shift from zygomorphy to actinomorphy in the mutants.

To determine whether the up-regulation of CYC-like expression levels leads to the dorsalized flowers observed in the mutants, we chose MlCYC2A for overexpression using the cauliflower mosaic virus (CaMV) 35S promoter in LF10 wild-type background, due to the known functional redundancy of CYC paralogs in M. lewisii (36). As expected, the transgenic lines with high MlCYC2A expression levels exhibited completely dorsalized flowers as seen in the three independent representative transgenic lines with similar floral phenotypes (Fig. 2, H and I). However, it is important to note that many differences were also observed between the floral phenotypes of the ML14181/ML14132 mutants and the 35S: MlCYC2A transgenic lines. The mutants displayed extra floral organs and partial homeotic transformations, which were not observed in the 35S: Ml-CYC2A transgenic lines, suggesting that the mutant likely regulates an array of additional genes related to flower development, in addition to MlCYC2A and MlCYC2B.

The ortholog of *Arabidopsis BLADE-ON-PETIOLE* is mutated in ML14181

To identify the gene responsible for the ML14181 mutant phenotypes, we conducted a bulk segregant analysis and compared single-nucleotide polymorphism (SNP) profiles of several previously reported EMS mutants (table S2). This analysis revealed a single sharp peak at the end of chromosome 8 (Fig. 2J), which corresponds to the gene encoding the Arabidopsis BLADE-ON-PETIOLE (BOP) homolog in Mimulus (fig. S3). BOP contains two conserved protein-protein interaction motifs: a BTB/POZ (for Broad Complex, Tramtrack, and Bric-a-brac/POX virus and Zinc finger) domain at the N terminus and four ankryin motifs near the C terminus (27). The identified gene in ML14181 contains a nonsynonymous substitution, leading to a histidine-to-leucine replacement (H39L; Fig. 2K). Notably, this H residue at position 39 is highly conserved in all protein species containing a BTB/POZ domain across plants, animals, and fungi (37, 38). We reasoned that this H39L replacement is likely to disrupt protein function, making BOP the most promising candidate underlying the mutant phenotype.

Further analysis of the BOP coding sequence (CDS) from ML14132 and NJ01339 mutants through Sanger sequencing revealed independent mutations. The ML14132 mutant carried a nonsynonymous substitution of serine-to-proline (S402P; Fig. 2K) neighboring the ankryin repeat motif. Notably, NJ01339 had the exact same position being mutated as ML14132, but with a nonsynonymous substitution of serine-to-leucine (S402L, Fig. 2K), further highlighting the importance of this residue. Together, the three independent mutations strongly support BOP as the causal gene responsible for the mutant phenotypes. Hence, we renamed the ML14181, ML14132, and NJ01339 mutants as bop-1, bop-2, and bop-3, respectively. To further validate the function of BOP, we performed a CRISPR-Cas9-mediated knockout of the BOP in M. verbenaceus. The resulting frameshift mutations in BOP closely resembled the bop-3 mutant phenotypes (Fig. 3, A and C). The two targeted mutations do not complement the *bop-3* mutant phenotypes, confirming that they are allelic (Fig. 3B).

To further confirm that *BOP* is the causal gene underlying the mutants, we attempted to complement the *bop-1* mutant with a wild-type *BOP* transgene. However, because of severe pistil development

impairment in the mutant, we circumvented this by first overexpressing the *MlBOP* driven by *35S* promoter in the wild-type background and then crossing this transgene into the *bop-1* mutant background. As expected, the transgene rescued the *bop-1* mutant phenotype, confirming that *BOP* is the causal gene. Similarly, introducing *35S*: *YFP-MlBOP* transgene into the *bop-3* background rescued the *bop-3* mutant phenotypes (fig. S4), further confirming that the observed mutant phenotypes are due to the loss of *BOP* function.

Spatiotemporal expression of MIBOP overlaps with MICYC2A

To explore the regulatory relationships between *MlBOP* and *MlCY-C2A*, we traced the expression patterns of both genes in LF10 with in situ hybridization assay. *MlBOP* exhibited early expression at the junctions between the floral meristem and the shoot apical meristem (two consecutive sections in Fig. 3D). As the floral meristem develops, *MlBOP* expression became localized to the dorsal (adaxial) region of the floral meristem. Subsequently, *MlBOP* expression was spatially restricted to the two dorsal petals and stamens (Fig. 3, E to G), which provides a potential mechanism to explain the conversion of stamens to petaloid organs in the mutant. As flower buds further developed, *MlBOP* expression expanded to the lateral and ventral petals (Fig. 3H). This later expansion of the *BOP* expression was independently validated by our reverse transcription polymerase chain reaction (RT-PCR) analysis of the floral organs dissected from the LF10 and MvBL floral buds (fig. S2, C and D).

Similarly, the expression of *MlCYC2A* was detected in a few cells at the adaxial side of the floral meristem (Fig. 3I). As the floral meristem expanded, *MlCYC2A* expression was restricted to the adaxial side of the floral primordia (Fig. 3, J and K). With the emergence of petal and stamen primordia, *MlCYC2A* expression remained restricted to the two adaxial petal and stamen primordia (Fig. 3L). As floral organs continued to differentiate, *MlCYC2A* expression was retained only in the two dorsal petal primordia throughout further development (Fig. 3, L to O), which was also independently validated by our RT-PCR analysis (fig. S2, C and D). The expression pattern of *MlCYC2A* closely mirrored that of *MlBOP* at early developmental stages, suggesting that *MlBOP* might regulate *MlCYC2A*.

MIBOP physically interacts with MICYC2A and MICulline3a

In Arabidopsis, AtBOP2 has been reported as an E3 ubiquitin ligase complex to regulate PHYTOCHROME INTERACTING FACTOR 4 and LEAFY to regulate plant development (39, 40). The overlapping expression domains between MlBOP and MlCYC2A prompted us to speculate that MIBOP may function as a putative member of a CUL3^{BOP} E3 ubiquitin ligase complex to post-translationally modify MlCYC2A. To test this hypothesis, we conducted yeast twohybrid (Y2H) assays to examine the interactions between MlBOP, MICYC2A, and MICulline3a. The results indicated that MIBOP and MlCulline3a interacted weakly in yeast. Unexpectedly, the interaction between bop-1 and MlCulline3a appeared stronger (Fig. 4A). We also found that bop-1 forms homodimers in yeast. However, we were not able to test this for the wild-type MIBOP because of its self-activation in yeast cells. In addition, we found that MICYC2A and MICYC2B can form homodimers and heterodimers as previously reported in other species (fig. S5) (41). We found that both MIBOP and bop-1 can interact with MICYC2A and MICYC2B, and bop-1 appears to interact stronger with MlCYC2A and MlCYC2B than MIBOP in yeast (Fig. 4A and fig. S5). The interaction between

Fig. 3. Functional characterization of the BOP in M.verbenaceus and in situ hybridization of MIBOP and MICYC2A in the wildtype LF10 background. (A) Flower phenotypes of the two independent BOP CRISPR-Cas9 knockout lines. Scale bars, 10 mm. (B) Flower phenotypes of the complementation crosses between the two CRISPR lines and the bop-3 mutant. Scale bars, 10 mm. (C) Illustrations of two independent CRISPR alleles relative to the guide RNA position in MvBOP. (D to H) Spatiotemporal expression pattern of MIBOP in LF10 flower buds at different developmental stages. Inflorescence meristems (IM) of different developmental stages in the scanning electron micrograph [(D), left] are labeled with an asterisk. Leaf primordia are blue color-coded. Two tiny IMs are demarcated with crescents. Two medium IMs are green color-coded. The adaxial side of the two large IMs is red color-coded. The yellow circle demarcates shot apical meristem. Note that the cross section in (E) is slightly tilted toward the adaxial side. (I to O) Spatiotemporal expression pattern of MICYC2A in LF10 flower buds at different developmental stages.

MlBOP, bop-1, and MlCYC2A was further confirmed in a pull-down assay. Consistently, bop-1 seems to be able to pull-down a larger quantity of MlCYC2A than MlBOP, suggesting that bop-1 interacts stronger with MlCYC2A than MlBOP (Fig. 4B). To further confirm these interactions in planta, we used a bimolecular fluorescence complementation (BiFC) assay (Fig. 4C). However, we were

not able to compare the affinities between the MlBOP-MlCYC2A and bop-MlCYC2A directly as the intensity of the fluorescence signal is difficult to compare across different experiments. Therefore, we used surface plasmon resonance (SPR) assay to measure the binding affinities [dissociation constant $(K_{\rm d})$] of the MlBOP-MlCYC2A and bop-1-MlCYC2A complexes in real time. The SPR

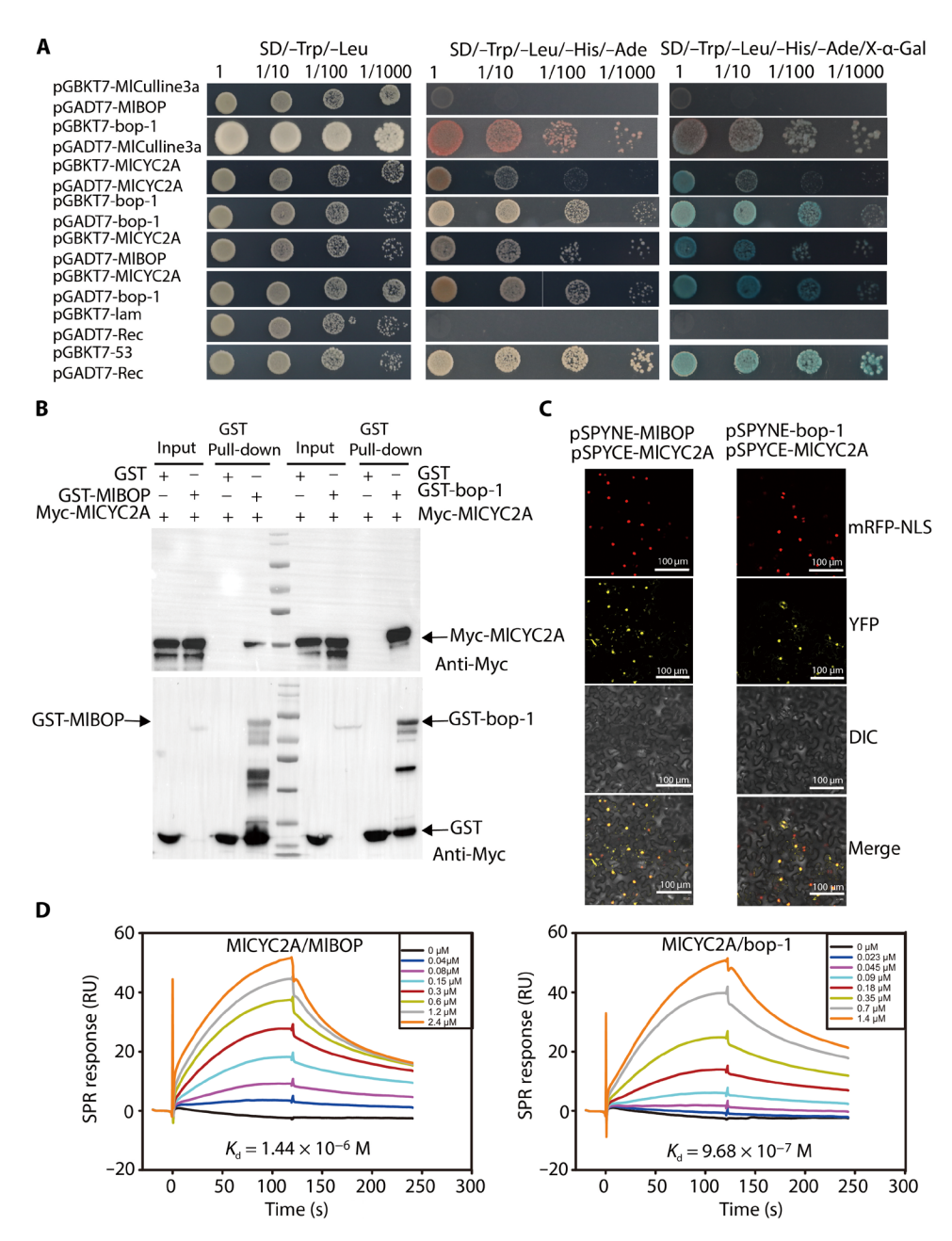


Fig. 4. MIBOP interacts with MICulline3a and MICYC2A to form a protein complex. (A) Interaction between MICYC2A or MICulline3a and MIBOP in yeast cells. SD/–Trp/–Leu indicates Trp and Leu synthetic dropout medium; SD/–Trp/–Leu/–His/–Ade indicates Trp, Leu, His, and Ade synthetic dropout medium. X-α-Gal, 5-Bromo-4-chloro-3-indolyl-α-p-galactopyranoside. (B) Interaction between MIBOP or bop-1 and MICYC2A in an in vitro pull-down assay. In vitro-translated GST protein was used as the negative control. "Input" indicates protein mixtures before the experiments and "Pull-down" indicates purified protein mixture. "+" indicates presence and "-" indicates absence. (C) Interaction between MIBOP or bop-1 and MICYC2A in BiFC assay. mRFP-NLS, nuclear marker coexpressing the 355:D53-RFP construct; YFP, images obtained in the yellow fluorescence channel; DIC, images obtained in bright light; and Merged, overlay plots. (D) SPR sensorgrams demonstrating the interaction of MIBOP or bop-1 with immobilized MICYC2A at different concentrations. Different colors show different concentrations of the partner protein, MIBOP or bop-1. The equilibrium dissociation constant (K_d) value is displayed under each sensorgram, respectively.

assay revealed that the $K_{\rm d}$ of the bop-1-MlCYC2A complex was stronger ($K_{\rm d}=9.68\times10^{-7}$ M) than that of the MlBOP-MlCYC2A complex ($K_{\rm d}=1.44\times10^{-6}$ M) (Fig. 4D), which is consistent with our Y2H and pull-down results.

We found that the protein-protein interaction between the orthologs of BOP and CYC in the selected species representing different clades of angiosperms is highly conserved: In the two species of Asterids we assayed, we found that AmBOP interacted with both CYC and DICH in snapdragon and CsBOP interacted with some but not all of the CYCs in chrysanthemum, suggesting the functional diversification of CYC after gene duplication in this lineage; In Arabidopsis (Rosids), both AtBOP1 and AtBOP2 interacted with AtTCP1, despite that it bears a radial symmetrical flower; we also found that DaBOP1 and DaBOP2 interacted with DaCYC2b in Delphinium anthriscifolium, which belongs to the basal eudicots. Furthermore, we detected the interaction between CeBOP1/2 and CeCYC1/2/3 in Cymbidium ensifolium (monocot) (fig. S6, A and C). Together, this suggests that BOP-CYC module is highly conserved in monocots and eudicots, and the diversification of floral symmetry in different lineages is likely due to the modification of this module or the downstream genes it targets. Intriguingly, BOP from different species interacted with MlCYC2B from Mimulus (fig. S6B), despite that some of them did not interact with the corresponding CYC encoded by their own genomes, highlighting the conservative roles of BOP as a pleiotropic regulator of plant development, whereas CYC is less pleiotropic, therefore, more prone to the modification of gene function.

MICYC2A functions as a competitor for ubiquitination of MIBOP

To determine whether MlCYC2A can be directly ubiquitinated by the MlCulline3a-MlBOP complex, we conducted in vitro ubiquitination assays and reconstituted the MlCulline3a-MlBOP-mediated ubiquitination cascade in *Escherichia coli*. Unexpectedly, MlCYC2A was either a poor substrate for ubiquitination or unable to be ubiquitinated by the putative MlCulline3a-MlBOP ligase complex [fig. S7, A and B; output part, anti-maltose-binding protein (MBP)]. Intriguingly, the presence of MlCYC2A notably reduced the amount of ubiquitination without MlBOP (fig. S7B, lane 5 versus 1, and lane 7 versus 6, anti-FLAG), indicating that MlCYC2A may act as a competitor, attenuating the ubiquitination catalyzed by the MlCulline3a-MlBOP ligase complex.

Moreover, the in vitro ubiquitination assay showed some ubiquitination occurred in the presence of only E1, E2, E3, and MlCulline3a (fig. S7B, lane 1, anti-FLAG), but the extent of ubiquitination was enhanced in the presence of MlBOP, and reduced when bop-1 was present (fig. S7B, lane 6 versus 1, and lane 8 versus 1, anti-FLAG), suggesting that MlBOP can be self-ubiquitinated. Together, these results suggest that MlCYC2A is unlikely to be a substrate for the MlCulline3a-MlBOP complex, and the mutation in the BTB domain plays a critical role in MlBOP self-ubiquitination.

MIBOP and MICYC2A competitively regulate the self-activation of MICYC2A

Our in vitro assays revealed intriguing regulatory relationships between MlBOP and MlCYC2A. Contrary to our initial hypothesis, MlBOP does not seem to ubiquitinate MlCYC2A. Instead, we found that MlCYC2A functions as an inhibitor of MlBOP self-ubiquitination, potentially modulating MlBOP homeostasis. This

discovery led us to explore alternative regulatory mechanisms between MlBOP and MlCYC2A.

We first isolated the promoter of *MlCYC2A* (~3 kb) in LF10 and identified a putative cis-element (P1: GGNCCCNC) matching the consensus CYC-like binding site (42). Our electrophoretic mobility shift assay (EMSA) and DNA-protein pulldown assay demonstrated that MlCYC2A specifically binds to this P1 element in the *MlCYC2A* promoter in vitro, while MlBOP does not (Fig. 5, A and B), lanes 3 and 4, output, anti-MBP). The specificity of MlCYC2A binding to the P1 element was further confirmed through a yeast one-hybrid (Y1H) assay (Fig. 5D) and a chromatin immunoprecipitation (ChIP)–PCR assay using flower buds of stably overexpressing *MlCYC2A* plants (Fig. 5E). These results indicate that MlCYC2A self-activates its own transcription by directly binding to the P1 element in the promoter.

Next, we investigated whether the interaction between MIBOP and MICYC2A could influence the binding of MICYC2A to the P1 element. Through a DNA-protein pulldown assay, we found that the presence of MIBOP reduced the amount of MICYC2A bound to the P1 element (Fig. 5B, lane 4 versus lane 5), indicating that the interaction between MlBOP and MlCYC2A interferes with MlCYC2A binding to its promoter. As an increasing amount of MIBOP was added to MlCYC2A, less P1 element was detected in vitro (Fig. 5C), indicating that MIBOP specifically inhibits the self-activation of Ml-CYC2A in a dose-dependent manner. To further test the repression of MICYC2A self-activation by MIBOP in planta, we conducted a dual-LUC assay on the same promoter used in the Y1H assay, in Nicotiana benthamiana leaves (Fig. 5F). We found that compared with the control (coinfiltration of empty plasmid with *pMlCYC2A*: LUC), the coexpression of 35S: MlCYC2A with pMlCYC2A: LUC had significantly increased the LUC:REN ratio. By contrast, the coexpression of 35S: MlBOP with pMlCYC2A: LUC did not significantly change the LUC:REN ratio, which is consistent with the lack of a DNA binding domain in MlBOP. The coexpression of 35S: MICYC2A and 35S: MIBOP with pMICYC2A: LUC had a similar LUC:REN ratio, indicating that MIBOP can indeed interfere with the transcriptional self-activation of *MlCYC2A* in planta.

Together, our findings suggest that MlBOP and MlCYC2A competitively regulate the self-activation of MlCYC2A by directly binding to the P1 element in the *MlCYC2A* promoter. The interaction between MlBOP and MlCYC2A appears to modulate the ability of MlCYC2A to activate its own transcription, resulting in a finely tuned regulatory mechanism that influences flower symmetry in *Mimulus*.

DISCUSSION

Flower symmetry is a crucial evolutionary innovation in angiosperms, and understanding the molecular and developmental mechanisms underlying this trait has been advanced through studies on model organisms like *Antirrhinum majus*. While the spatiotemporal expression pattern of *CYC* has been linked to flower symmetry in various plants (7, 8, 16, 35, 43–45), the regulatory mechanisms governing *CYC* expression have remained elusive. In this study, we used chemical mutagenesis and functional analysis to identify *BOP* as the causal gene underlying the floral symmetry mutants in *Mimulus*. Our in situ hybridization analysis revealed that the spatial and temporal expression of *MlBOP* overlaps with *MlCYC2A*, and probably *MlCYC2B*, suggesting a potential direct regulation of *MlCYC2A* and

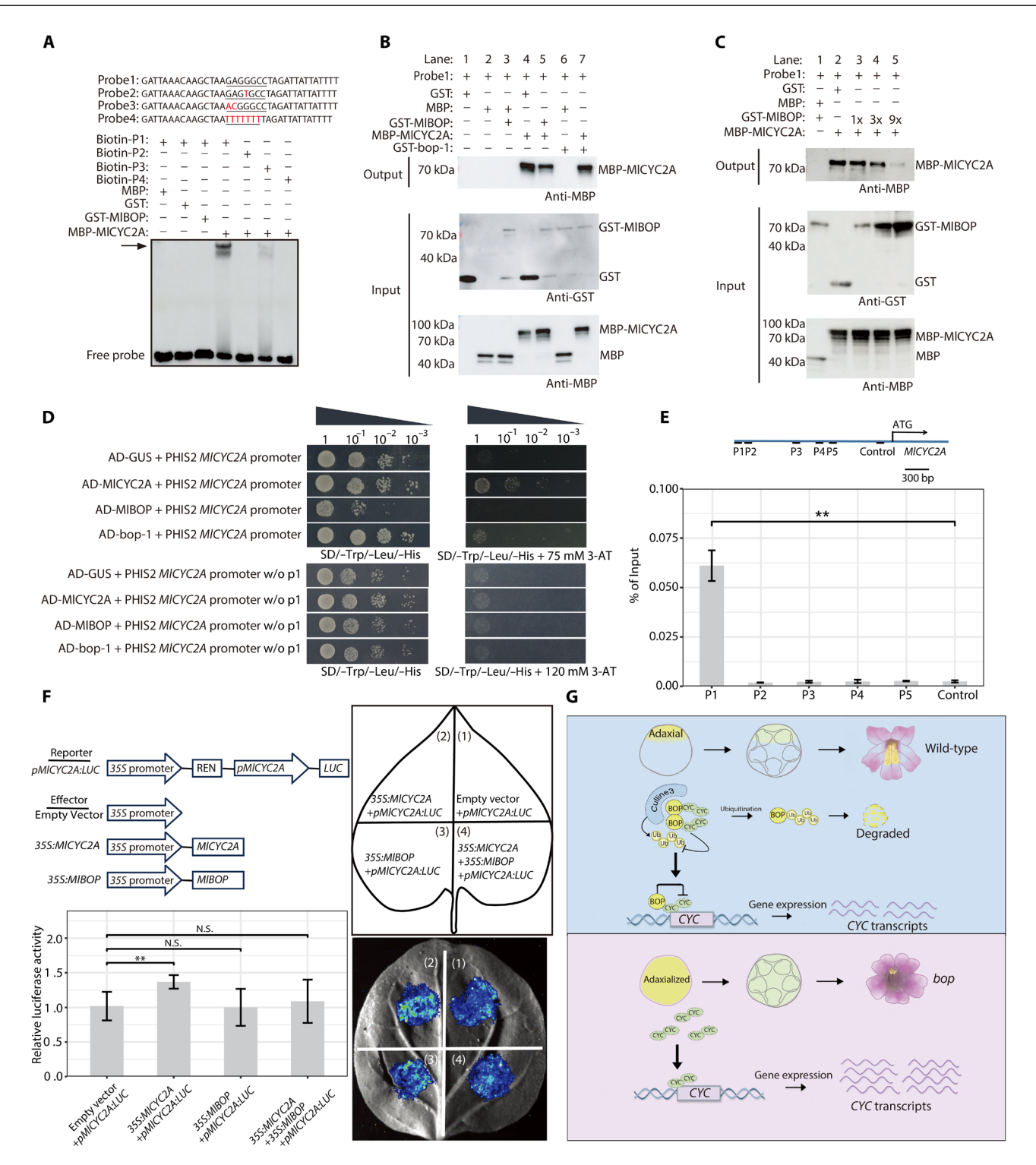


Fig. 5. MIBOP interacts with MICYC2A to modulate the self-activation of MICYC2A. (A) EMSA of interaction between MICYC2A, MIBOP, and putative MICYC2A binding sites. (B) DNA-Protein pulldown assays with the biotinylated P1 element from MICYC2A promoter with purified GST-tagged MIBOP or MBP-tagged MICYC2A. GST and MBP alone served as negative controls and inputs as a loading control. (C) MIBOP inhibits the binding of MICYC2A to the P1 element in a dose-dependent manner. GST and MBP alone were served as negative controls and inputs as a loading control. (D) Y1H assay showing MICYC2A specifically binds to the DNA fragment containing the P1 element. Both AD-GUS and AD-bop-1 were used as negative controls. (E) ChIP-PCR assay showing MICYC2A binding to the MICYC2A promoter in planta. Top: Schematic representation of the MICYC2A promoter. The blue line represents the entire length of the MICYC2A; the lines below are the fragments amplified in the ChIP-PCR assay. P1: -2796 to -2676 bp, P2: -2661 to -2560 bp, P3: -1796 to -1660 bp, P4: -1379 to -1275 bp, P5: -1119 to -1015 bp, Control: -263 to -98, relative to the MICYC2A translation initiation codon (ATG). Bottom: ChIP enrichment of the indicated MICYC2A promoter fragments (P1 to P5). ChIP samples were prepared using the anti-green fluorescent protein antibody. Error bars represent 1 SD from three biological replicates. (F) Dual-luciferase assay showing transactivation of the MICYC2A promoter by MICYC2A or MIBOP. Top left: Schematic representation of the obacco leaves infiltrated with different constructs. Bottom right: A representative transfection experiment result is shown. Bottom left: Statistical analysis of the LUC/REN value among different constructs infiltrated. Error bars represent 1 SD from seven biological replicates. Analysis of variance (ANOVA) test, **P < 0.01. (G) A model for the development of flower symmetry by the intricate molecular interaction between BOP and CYC.

MICYC2B by MIBOP. However, because MIBOP lacks a DNA binding domain, direct binding to the MlCYC2A promoter is unlikely. Our in vitro assays indicated that MIBOP interacts with both MlCulline3a and MICYC2A, forming a potential ubiquitination complex to target MICYC2A for degradation. Unexpectedly, MICYC2A was not ubiquitinated by MIBOP in our in vitro ubiquitination assays. Instead, MIBOP was found to be self-ubiquitinated, modulating its own homeostasis. We further demonstrated that MICYC2A selfregulates and that MIBOP functions as a modulator to fine-tune this MICYC2A-mediated feedback regulatory loop. This regulatory loop is further complicated by the possible involvement of MlCYC2B, which might cross-regulate MlCYC2A, and vice versa (42). This reveals a highly sophisticated and intricate regulatory relationship between BOP and CYC in Mimulus (Fig. 5G). Given the similarity in spatiotemporal patterns of the MlCYC2A with those in Antirrhinum and other plants (8, 14, 16, 17, 20) and the conservative proteinprotein interaction between BOP and CYC in many different lineages, this mechanism is likely highly conserved in angiosperms. One particularly intriguing observation from our data is that the ability of BOP to interact with CYC seems to be highly conserved, as all of the BOP proteins tested interacted with the MICYC2B from Mimulus, but some of them failed to interact with the cognate CYC proteins encoded by their own genomes. Because BOP regulates an array of plant developmental processes, whereas CYC is more specific to flower development, evolution must have exerted a strong selective pressure on BOP, with less constraint on CYC. Whether this module predates the evolution of the basal angiosperms warrants further investigations by sampling basal angiosperm species. Our findings suggest that evolutionary shifts in flower symmetry across many clades might not necessarily involve direct changes of CYC alone but could potentially be influenced by molecular modifications involving BOP and its interacting partners or its downstream targets.

One question that remains to be addressed is the peculiar expansion of MlCYC2A across the flower in the bop mutant. If the interaction between MIBOP and MICYC2A functions to fine-tune the expression of MlCYC2A, we would expect the up-regulation of Ml-CYC2A in the dorsal petals rather than its expansion across the flower in the mutant. We hypothesize that MlBOP may initially trigger a signal to regulate the adaxial-abaxial polarity of the inflorescence meristem (IM), a process reminiscent of establishing discrete adaxial and abaxial domains of leaf primordium. Following the onset of the IM polarity, the two dorsal petal primordia initiate in the adaxial domain, and MIBOP interacts with MICYC2A to maintain the expression of MlCYC2A. However, in the bop mutant, the IM polarity is adaxialized. All petal primordia gain a dorsal petal identity as a result, leading to the expansion of MlCYC2A. Despite that the molecular identity of this initial signal remains obscure, auxin is a prime candidate: First, it has been shown that applying auxin or auxin transport inhibitor in snapdragon (46) and Mimulus (24) can change the flower symmetry, suggesting that auxin is involved in the regulation of flower symmetry. Second, in Arabidopsis, BOP has been shown to regulate an array of leaf polarity regulators (47), which are known to modulate the spatial pattern of auxin signaling (48). Third, it has been shown in snapdragon that flower symmetry can response to the dorsoventral prepattern (49). Our model predicts the expansion of the adaxial regulators such as AS1, AS2, HD-ZIPIII, and auxin signaling in the bop mutant IM (Fig. 5G). These hypotheses can be directly tested by tracing the expression of these genes or by manipulating their functions in the early developmental stages of IM in future studies.

MATERIALS AND METHODS

Plant materials and growth conditions

The *M. lewisii* inbred line LF10 was previously described (50). EMS mutants were generated using *M. lewisii* LF10 and *M. verbenaceus* following Owen and Bradshaw (51). Plants were grown in the University of Connecticut research greenhouse and Nanjing Agricultural University research greenhouse under natural light supplemented with sodium vapor lamps and light-emitting diode lights, respectively, ensuring a 16-hour day length.

Genomic analyses for causal gene identification

To identify the causal gene underlying the ML14181, we used a hybrid strategy that combines the advantages of bulk segregant analysis and genome comparisons between multiple EMS mutants, as described previously (52). Briefly, for the ML14181 mutant, an F₂ population was produced by crossing the homozygous mutant (generated in the LF10 background) and the mapping line SL9. DNA samples from 96 F₂ segregants displaying the mutant phenotype were pooled with equal representation. A small-insert library was then prepared for the pooled sample and was sequenced using an Illumina HiSeq 2000 platform at the University of North Carolina High Throughput Sequencing Facility. These short reads were then mapped to the LF10 genome assembly version 2.0 (http://monkeyflower.uconn.edu/resources/) using CLC Genomics Workbench 7.0 (Qiagen, Valencia, CA). After comparisons to the SNP profiles of previously published mutants, guideless (53), rcp1 (54), act1-D (55), and rcp2 (56), we narrowed the causal mutation to a single candidate SNP for ML14181. The allelic ML14132 and NJ01339 mutants were sequenced by Sanger sequencing to detect the mutations.

Expression analysis by RT-qPCR

Total RNA was isolated from specified floral tissues using a Quick RNA isolation kit (Huayueyang Biotechnology, Beijing, China) following the manufacturer's instructions and treated with ribonuclease-free deoxyribonuclease (Vazyme Biotech Co. Ltd., Nanjing, China) to avoid genomic DNA contamination. Reverse transcription was performed to synthesize cDNA from 1 μg of total RNA using the HiScript II Q Select RT SuperMix (Vazyme Biotech Co. Ltd., Nanjing, China) following the manufacturer's instructions. Next, cDNA samples were diluted 20-fold before RT-qPCR. All RT-qPCRs were performed using the TB Green Premix Ex Taq II (Tli RNaseH Plus) (Takara, Dalian, China) in a CFX96 Touch Real-Time PCR Detection system (Bio-Rad, USA). Samples were amplified for 50 cycles for 95°C for 15 s and 60°C for 30 s. MlUBC was used as a reference gene to normalize expression levels following the $\Delta\Delta$ Ct method (50).

Plasmid construction and plant transformation Overexpression plasmids

To generate the 35S: MIBOP, 35S: MICYC2A, and 35S: YFP-MIBOP constructs, we first amplified the full-length CDS of MIBOP and MICYC2A from the wild-type LF10 cDNA using the Phusion enzyme (NEB, Ipswich, MA), respectively. For each gene, the amplified fragment was cloned into the pENTR/D-TOPO vector (Invitrogen), and then a linear fragment containing the CDS flanked by the attL1 and attL2 sites was amplified using M13 primers. The linear fragments of MIBOP and MICYC2A were subsequently recombined into the respective Gateway vector pEarleyGate 100 and pEarleyGate 101 (57), which drives transgene expression by the CaMV 35S promoter. The CDS of

MlBOP was recombined into the pEarleyGate 100 and 104 vector to complement the *M. lewisii* ML14181 mutant and *M. verbenaceus* NJ01339 mutant phenotypes, respectively.

CRISPR-Cas9 plasmid

To knock out the function of MvBOP, we undertook a targeted genome editing approach using the Cas9-single-guide RNA (sgRNA) system to recapitulate the BOP loss-of-function phenotype in M. verbenaceus. Four sgRNA guides were designed to target the first exon of MvBOP (sgRNA1:TCAGCGTAGAGGGTCGTCTC; sgRNA2: CAGCTCGGAGCCTCTTCTTC; sgRNA3:GAGCTCCGACCCGT TGAGGA; sgRNA4:CTCGCCGCCGCTAGATCCTT). The 20-bp guide sequences were further verified for their specificity by using a blast algorithm to scan the M. verbenaceus v2.0 reference genome (http://mimubase.org/). The sgRNAs were cloned into sgRNA expression cassettes using overlapping PCR and then ligated by the Golden Gate cloning methods into the binary vector pYLCRISPR/ Cas9P35S-B (Addgene no. 66190) for multiplex gene editing following the previously described protocol (58). For genotyping of the transgenic plants, leave tissues of the transgenic plants were collected from each plant, and genomic DNA was isolated using the Cetyltrimethylammonium Bromide (CTAB) method. PCR amplification was performed using primers flanking the full length of the BOP, and Sanger sequencing was used to identify mutations in the MvBOP transgenic plants. All plasmids were verified by sequencing before being transformed into Agrobacterum tumefaciens strain GV3101 for subsequent stable plant transformation, as previously described (50).

RNA in situ hybridization

Probe synthesis was performed on cDNA using gene-specific primers (table S3) and labeled with DIG RNA Labeling Kit (catalog no. 11175025910, Roche Diagnostics GmbH, Mannheim, Germany). Other steps were performed as previously described (59). Results were visualized in the Central Laboratory of the College of Horticulture on a Leica DM6 B Upright Microscope using a bright field.

Y2H assay

Y2H constructs were built using the Matchmaker Gold Y2H system (Clontech). The full-length CDSs of MlCulline3a, MlBOP, bop-1, MlCYC2A, and MlCYC2B from M. lewisii, AtBOP1, AtBOP2, and AtTCP1 from Arabidopsis thaliana, AmBOP, AmCYC, and Am-DICH from A. majus, CsBOP, CsCYC2a1, CsCYC2a2, CsCYC2c, CsCYC2d, CsCYC2e, and CsCYC2f from Chrysanthemum seticuspe, DaBOP1, DaBOP2, DaCYC2a, and DaCYC2b from D. anthriscifolium, and CeBOP1, CeBOP2, CeCYC1, CeCYC2, and CeCYC3 from C. ensifolium were separately recombined into the pGBKT7-BD bait vector, and the pGADT7-AD prey vector using an In-Fusion cloning kit (Clontech). The resultant preys and baits were then cotransformed into Saccharomyces cerevisiae strain Y2H using the lithium acetate method. After inoculating on a selective medium lacking Trp and Leu (-T/-L), the positive colonies were inoculated on a selective medium lacking Trp, Leu, His, and adenine (-L/-T/ −H/−A) and grown for 2 days at 28°C, which were further subjected to X-α-Gal, to identify possible interactions. pGBKT7-53 and pGADT7-Rec were used as positive controls and pGBKT7-lam and pGADT7-Rec were used as negative controls.

In vitro pull-down assay

To test whether MIBOP and bop-1 interact with MICYC2A, respectively, the CDS of *MIBOP* was cloned by PCR amplification and inserted into the pGEX-5X-1 vector using Bam HI and Not I sites to generate plasmid expressing glutathione *S*-transferase (GST)–tagged

MlBOP. A point mutation of *MlBOP* (H39L) was generated using the QuickMutation site-directed mutagenesis kit (Beyotime, China) to create a plasmid expressing GST-tagged MlBOP with the H39L point mutation (bop-1). *MlCYC2A* CDS was cloned by PCR amplification fused with Myc tag (EQKLISEEDL) in N terminus and inserted into the pET21b vector using Hind III site to generate plasmid expressing Myc-tagged MlCYC2A.

Myc-MlCYC2A, GST-MlBOP, GST-bop-1, and GST empty vector were individually expressed in E. coli BL21 (DE3) cells. Wholecell lysates (WCL) from E. coli BL21 overexpressing MYC-MlCYC2A, GST-MIBOP, GST-bop-1, or GST alone were extracted by ultrasonic with lysis buffer containing 20 mM tris-HCl (pH 7.5), 200 mM NaCl, 1 mM EDTA, 1x cocktail of protease inhibitors, and 1 mM PMSF (phenylmethylsulfonyl fluoride, Sigma-Aldrich). WCL expressing recombinant GST-tag fusion and MYC-tag fusion proteins were mixed in equal amounts and purified with glutathione magnetic agarose beads (Thermo Fisher Scientific, Shanghai, China), washed three times by lysis buffer, separated by 10% SDS-polyacrylamide gel electrophoresis (SDS-PAGE), transferred onto polyvinylidene difluoride (PVDF) membranes (Millipore, USA), and subjected to Western blotting following standard protocols. Eluted proteins were probed with anti-MYC (Abmart, China) antibody to identify possible interactions. A similar procedure was followed to test the interaction between AtBOP1 or AtBOP2 and AtTCP1 in an in vitro pull-down assay.

BiFC assay

For BiFC assays, the CDSs of *MlBOP* and *bop-1* were cloned into the pSPYNE vector, respectively; while the CDS of the *MlCYC2A* was cloned into the pSPYCE vector (60). The resultant vectors were introduced into *Agrobacterium tumefaciens* strain EHA105, and then transiently coinfiltrated in *N. benthamiana* leaves following Ding and Yuan (61). The coexpressed 35S: D53-RFP construct was used as a nuclear marker and visualized by fluorescence microscopy. Fluorescence images were acquired using a high-resolution confocal laser microscope (ZEISS, LSM800) in the Central Laboratory of the College of Horticulture, Nanjing Agricultural University.

SPR analysis

SPR experiments were performed using the BIAcore T-200 system at room temperature to quantitatively characterize the binding affinity between the MICYC2A and MIBOP, MICYC2A and bop-1. MICYC2A CDS was cloned by PCR amplification and inserted into the pMBP-C vector using Bam HI and Nhe I sites to generate plasmid expressing MBP-tagged MICYC2A. MBP-MICYC2A was generated from *E. coli* BL21 (DE3) cells and purified using Dextrin Resin 6FF (Sangon Biotech, Shanghai, China) according to the manufacturer's protocol. GST-MIBOP and GST-bop-1 proteins were purified as mentioned above. MBP-MICYC2A was immobilized on the CM5 sensor chips (GE Healthcare) via amine coupling. Serially diluted MIBOP/bop-1 proteins in Hepes buffer [0.01 M Hepes, 0.15 M NaCl, 0.5% surfactant P20, and 3 mM EDTA (pH 7.4)] were followed over the chips. The kinetic data were analyzed with the Biacore T200 Evaluation software using the steady-state affinity model.

E. coli-based ubiquitination assay

To test whether MlCYC2A can be directly ubiquitinated by MlBOP, we performed an in vitro ubiquitination assay with a reconstituted *E. coli* system. The ubiquitination reaction was carried out according to the

previously described principle of reconstituting the basic ubiquitination cascade in E. coli (62). To reconstitute the complex, CUL3-mediated ubiquitination cascade, the reaction components consisting of a total of seven proteins (MlCYC2A, MlBOP, CUL3, RBX1, E1, E2, and Ubiquitin) were coexpressed in E. coli using a modified Duet vector system (Novagen). Details of the plasmid pACYCDuet-1:RBX1 + Myc-CUL3 (pACYC-RC3); pCDFDuet-1:HA-Ub + UBC8 + UBA1 (pCDF-Ub) and pETDuet-1:Flag-WRKY70 + GST (pET-AdS) were described in a previous study (63). Six derivations of pET-AdS plasmid were constructed in this study, including different control plasmids. The CDS of MICYC2A fused to the MBP tag or MBP tag alone was amplified by PCR and inserted between Nco I and Not I in MCS-1 of the pETDuet-1: Flag-WRKY70 + GST to generate the pETDuet-1: MBP-MlCYC2A + GST and pETDuet-1: MBP + GST. The CDSs of MlBOP or bop-1 fused to GST, were amplified and inserted between NdeI and AvrII in MCS-II of the pETDuet-1: MBP-MICYC2A + GST and pETDuet-1: MBP + GST to generate pETDuet-1: MBP-MICYC2A + GST-MIBOP/bop-1 and pETDuet-1: MBP + GST-MIBOP/bop-1. The three vectors, pET-AdS, pACYC-RC3 and pCDF-Ub, were cotransformed into the E. coli strain BL21 (DE3) and ubiquitination reaction was initiated by inducing protein expression with 0.5 mM IPTG for 3 hours at 28°C. Proteins were extracted by ultrasonic with lysis buffer containing 20 mM tris-HCl (pH 7.5), 200 mM NaCl, 1 mM EDTA, 1× cocktail of protease inhibitors, and 1 mM PMSF (phenylmethylsulfonyl fluoride, Sigma-Aldrich). The expression of proteins was confirmed with SDS-PAGE on the total lysate. To detect ubiquitination of MBP-MlCYC2A under denaturing conditions, 1% SDS was added to the lysate and heated at 95°C for 10 min, then diluted 10 times with the lysis buffer and subjected to immunoprecipitation (IP) using a-Dextrin Resin 6FF beads (Sangon Biotech, Shanghai, China). Eluted proteins were subjected to 10% SDS-PAGE and probed with anti-MBP (Transgen, China) and Anti-HA (Invitrogen, USA) antibodies.

In vitro ubiquitination assay

GST-MIBOP, GST-bop-1, MBP-MICYC2A, MBP, and GST proteins were individually expressed in E. coli strain BL21 (DE3) and purified with glutathione magnetic agarose beads (for the GST tag, Thermo Fisher Scientific, Shanghai, China) or Dextrin Resin 6FF beads (for the MBP tag, Sangon Biotech, Shanghai, China). The recombinant human ubiquitin-activating enzyme (UBE1), ubiquitin-conjugating enzyme (UbcH5b), and Cullin3/Nedd8/Rbx1 recombinant proteins were purchased from R&D systems (R&D Systems, USA). Ubiquitination reactions were performed as described previously with slight modification (39). UBE1 (100 nM), 1 mM UbcH5b, 100 nM Cullin3/Nedd/Rbx1, 1 µM GST-MlBOP, and 1 µM MBP-MlCYC2A were incubated at 30°C for 2 hours in a buffer containing 5 µg of flag-ubiquitin, 50 mM tris-HCl (pH 7.5), 50 mM NaCl, 5 mM MgCl₂, 5 mM adenosine triphosphate, and 2 mM DTT. The reactions were stopped after 10 min at 95°C by boiling in DTT-containing SDS loading buffer, and proteins were resolved by 10% SDS-PAGE and immunoblotted. Anti-Flag antibodies were used for the detection of the ubiquitin. Anti-MBP antibodies were used for the detection of the MBP proteins. The reactions without E1, E2, or E3 and the reactions with MBP or GST were used as negative controls.

Electrophoretic mobility shift assay

GST-MIBOP, GST-bop-1, MBP-MICYC2A, MBP, and GST proteins were purified as mentioned above. Probes of 37-bp in length containing the binding site of the *MICYC2A* promotor were synthesized

and labeled with biotin at their 5' ends. The probes were also mutated to test the binding specificity of the proteins. Annealed double-stranded probes were incubated with the purified GST-MlBOP and MBP-MlCYC2A in binding buffer [10X Binding Buffer, 1 μ g/Poly(dI-dC)] for 30 min at 25°C. Purified GST-tagged MlBOP or MBP-tagged MlCYC2A was incubated with a 20 nM wild-type or mutated biotin-labeled probe. DNA-protein complexes were separated by nondenaturing PAGE on ice. EMSA was performed using the LightShift EMSA Optimization and Control Kit (Thermo Fisher Scientific, Shanghai, China) and Chemiluminescent Nucleic Acid Detection Module Kit (Thermo Fisher Scientific, Shanghai, China), following the manufacturer's instructions.

Y1H assay

For Y1H assays, the CDSs of *MlCYC2A*, *MlBOP*, and *bop-1* were inserted into the pGADT7 vector as preys. The promoter fragments of *MlCYC2A*, with or without the putative P1 element fragment were cloned into the pHIS2 vector as baits. After cotransformation of the prey and bait into the yeast strain *S. cerevisiae* Y187 using the lithium acetate method, the resultant yeast cells were plated onto a selective medium lacking Trp, Leu, and His (SD/–Trp/–Leu/–His). Subsequently, the positive colonies were inoculated on a Trp/–Leu/–His medium supplemented with an appropriate concentration of 3-AT and grown for 3 days at 28°C to identify possible interactions. The CDS of *GUS* (β-glucuronidase) was inserted into the pGADT7 vector as the negative control.

DNA-protein binding assay

GST-MIBOP, GST-bop-1, MBP-MICYC2A, MBP, and GST proteins were purified as mentioned above. Biotinylated DNA fragments corresponding to the *MICYC2A* promoter P1 element were generated by PCR. For DNA-protein pulldown, biotinylated P1 fragments were first incubated with streptavidin-bound magnet beads (Thermo Fisher Scientific, Shanghai, China) in binding buffer [50 mM tris-HCl (pH 7.5), 100 mM NaCl, 0.05% Nonidet P40, and 1 mM EDTA] for 2 hours at 4°C, then washed three times in binding buffer. Proteins were added to DNA-bound beads, and the mixture was rotated in a 4°C cold room for 2 hours. Beads were washed three times with binding buffer; proteins were stripped off the beads by boiling with 2× SDS buffer and then subjected to SDS-PAGE. The gel was transferred onto PVDF membranes (Millipore, USA), and subjected to Western blotting following standard protocols. Eluted proteins were probed with anti-MBP or anti-GST (Abmart, China) antibody to identify possible interactions.

ChIP-PCR assay

For ChIP assays, 1.5 g of ~2-mm flower buds of 35S: MICYC2A-YFP were cross-linked in polyformaldehyde. The chromatin was sheared to an average of 500 bp by sonication and immunoprecipitated with green fluorescent protein recombinant rabbit monoclonal antibody (Thermo Fisher Scientific). Subsequently, the enriched DNA fragments were examined by RT-qPCR.

Phylogenetic analysis

Multiple sequence alignment of BOP and related proteins was performed using AliView (64). To identify putative orthologous of CYC in Mimulus, CYC, DICH from snapdragon, and multiple related proteins from other species were aligned to perform phylogenetic analysis. Maximum likelihood analysis was conducted in MEGA (65) with the default setting, except for a bootstrap value of 10,000.

Dual-LUC reporter assay

For Dual-LUC reporter assay, the promoter fragment of *MlCYC2A* was cloned into the pGreenII 0800-LUC vector (66) to generate the reporter construct. The CDSs of the *MlBOP* and *MlCYC2A* were cloned into the *pORE-R4* vector (67) under the control of the 35S promoter to generate the effector constructs. Subsequently, the *A. tumefaciens* containing the reporter constructs and effector constructs, respectively, were transiently coinfiltrated in *N. benthamiana* leaves. The LUC-to-REN activity ratio was measured using the Infinite M200 luminometer (Tecan, Mannerdorf, Switzerland) with the Dual-Glo Luciferase Assay System (Promega, Beijing, China). All primers are listed in table S3.

Scanning electron microscopy

Flower buds were fixed overnight in formalin-acetic-alcohol at 4°C, dehydrated for 30 min through a 50, 60, 70, 95, and 100% alcohol series. Samples were then critical-point dried, mounted, and sputter coated before being observed using a NOVA NanoSEM with Oxford EDX at 35 kV at UConn's Bioscience Electron Microscopy Laboratory.

Supplementary Materials

This PDF file includes:

Figs. S1 to S7 Tables S1 to S3

REFERENCES AND NOTES

- J. P. Hunter, Key innovations and the ecology of macroevolution. Trends Ecol. Evol. 13, 31–36 (1998)
- P. K. Endress, Evolutionary diversification of the flowers in angiosperms. Am. J. Bot. 98, 370–396 (2011).
- P. Cubas, Floral zygomorphy, the recurring evolution of a successful trait. Bioessays 26, 1175–1184 (2004).
- M. J. Donoghue, R. H. Ree, D. A. Baum, Phylogeny and the evolution of flower symmetry in the Asteridae. Trends Plant Sci. 3, 311–317 (1998).
- G. L. Stebbins, Flowering Plants: Evolution above the Species Level (Belknap Press of Harvard University Press, 1974).
- P. K. Endress, Symmetry in flowers: Diversity and evolution. Int. J. Plant. Sci. 160, S3–S23 (1999).
- D. Luo, R. Carpenter, L. Copsey, C. Vincent, J. Clark, E. Coen, Control of organ asymmetry in flowers of Antirrhinum. Cell 99, 367–376 (1999).
- D. Luo, R. Carpenter, C. Vincent, L. Copsey, E. Coen, Origin of floral asymmetry in Antirrhinum. Nature 383, 794–799 (1996).
- S. B. Corley, R. Carpenter, L. Copsey, E. Coen, Floral asymmetry involves an interplay between TCP and MYB transcription factors in *Antirrhinum. Proc. Natl. Acad. Sci. U.S.A.* 102, 5068–5073 (2005).
- J. Raimundo, R. Sobral, P. Bailey, H. Azevedo, L. Galego, J. Almeida, E. Coen, M. M. R. Costa, A subcellular tug of war involving three MYB-like proteins underlies a molecular antagonism in *Antirrhinum* flower asymmetry. *Plant J.* 75, 527–538 (2013).
- J. Almeida, M. Rocheta, L. Galego, Genetic control of flower shape in Antirrhinum majus. Development 124, 1387–1392 (1997).
- L. Galego, J. Almeida, Role of DIVARICATA in the control of dorsoventral asymmetry in Antirrhinum flowers. Genes Dev. 16, 880–891 (2002).
- M. A. Chapman, S. Tang, D. Draeger, S. Nambeesan, H. Shaffer, J. G. Barb, S. J. Knapp, J. M. Burke, Genetic analysis of floral symmetry in Van Gogh's sunflowers reveals independent recruitment of CYCLOIDEA genes in the Asteraceae. *PLOS Genet.* 8, e1002638 (2012)
- H. L. Citerne, R. T. Pennington, Q. C. B. Cronk, An apparent reversal in floral symmetry in the legume Cadia is a homeotic transformation. *Proc. Natl. Acad. Sci. U.S.A.* 103, 12017–12020 (2006).
- L. C. Hileman, E. M. Kramer, D. A. Baum, Differential regulation of symmetry genes and the evolution of floral morphologies. *Proc. Natl. Acad. Sci. U.S.A.* 100, 12814–12819 (2003).
- X. Feng, Z. Zhao, Z. Tian, S. Xu, Y. Luo, Z. Cai, Y. Wang, J. Yang, Z. Wang, L. Weng, J. Chen, L. Zheng, X. Guo, J. Luo, S. Sato, S. Tabata, W. Ma, X. Cao, X. Hu, C. Sun, D. Luo, Control of petal shape and floral zygomorphy in Lotus japonicus. *Proc. Natl. Acad. Sci. U.S.A.* 103, 4970–4975 (2006).

- Z. Wang, Y. Luo, X. Li, L. Wang, S. Xu, J. Yang, L. Weng, S. Sato, S. Tabata, M. Ambrose,
 C. Rameau, X. Feng, X. Hu, D. Luo, Genetic control of floral zygomorphy in pea (Pisum sativum L.). Proc. Natl. Acad. Sci. U.S.A. 105, 10414–10419 (2008).
- S. K. Broholm, S. Tahtiharju, R. A. Laitinen, V. A. Albert, T. H. Teeri, P. Elomaa, A TCP domain transcription factor controls flower type specification along the radial axis of the Gerbera (Asteraceae) inflorescence. *Proc. Natl. Acad. Sci. U.S.A.* 105, 9117–9122 (2008).
- J. Zhong, J. C. Preston, L. C. Hileman, E. A. Kellogg, Repeated and diverse losses of corolla bilateral symmetry in the Lamiaceae. *Ann. Bot.* 119, 1211–1223 (2017).
- W. Zhang, V. W. Steinmann, L. Nikolov, E. M. Kramer, C. Davis, Divergent genetic mechanisms underlie reversals to radial floral symmetry from diverse zygomorphic flowered ancestors. Front. Plant Sci. 4, 302 (2013).
- X.-R. Zhou, Y.-Z. Wang, J. F. Smith, R. Chen, Altered expression patterns of TCP and MYB genes relating to the floral developmental transition from initial zygomorphy to actinomorphy in Bournea (Gesneriaceae). New Phytol. 178, 532–543 (2008).
- J. C. Preston, C. C. Martinez, L. C. Hileman, Gradual disintegration of the floral symmetry gene network is implicated in the evolution of a wind-pollination syndrome. *Proc. Natl. Acad. Sci. U.S.A.* 108, 2343–2348 (2011).
- L. C. Hileman, Trends in flower symmetry evolution revealed through phylogenetic and developmental genetic advances. *Philos. Trans. R. Soc. Lond. B Biol. Sci.* 369, 20130348 (2014)
- B. Ding, J. Li, V. Gurung, Q. Lin, X. Sun, Y.-W. Yuan, The leaf polarity factors SGS3 and YABBYs regulate style elongation through auxin signaling in *Mimulus lewisii*. New Phytol. 232, 2191–2206 (2021).
- M. Khan, H. Xu, S. R. Hepworth, BLADE-ON-PETIOLE genes: Setting boundaries in development and defense. Plant Sci. 215-216, 157–171 (2014).
- C. M. Ha, G.-T. Kim, B. C. Kim, J. H. Jun, M. S. Soh, Y. Ueno, Y. Machida, H. Tsukaya, H. G. Nam, The BLADE-ON-PETIOLE 1 gene controls leaf pattern formation through the modulation of meristematic activity in Arabidopsis. *Development* 130, 161–172 (2003).
- C. M. Ha, J. H. Jun, H. G. Nam, J. C. Fletcher, BLADE-ON-PETIOLE1 encodes a BTB/POZ domain protein required for leaf morphogenesis in Arabidopsis thaliana. *Plant Cell Physiol.* 45, 1361–1370 (2004).
- M. Jost, S. Taketa, M. Mascher, A. Himmelbach, T. Yuo, F. Shahinnia, T. Rutten, A. Druka, T. Schmutzer, B. Steuernagel, S. Beier, S. Taudien, U. Scholz, M. Morgante, R. Waugh, N. Stein, A homolog of Blade-On-Petiole 1 and 2 (BOP1/2) controls internode length and homeotic changes of the barley inflorescence. *Plant Physiol.* 171, 1113–1127 (2016).
- C. Xu, S. J. Park, J. Van Eck, Z. B. Lippman, Control of inflorescence architecture in tomato by BTB/POZ transcriptional regulators. *Genes Dev.* 30, 2048–2061 (2016).
- S. R. Hepworth, Y. Zhang, S. McKim, X. Li, G. W. Haughn, BLADE-ON-PETIOLE-dependent signaling controls leaf and floral patterning in Arabidopsis. *Plant Cell* 17, 1434–1448 (2005).
- J. R. Shoesmith, C. U. Solomon, X. Yang, L. G. Wilkinson, S. Sheldrick, E. van Eijden, S. Couwenberg, L. M. Pugh, M. Eskan, J. Stephens, A. Barakate, S. Drea, K. Houston, M. R. Tucker, S. M. McKim, APETALA2 functions as a temporal factor together with BLADE-ON-PETIOLE2 and MADS29 to control flower and grain development in barley. Development 148. 1–16 (2021).
- J.-M. Couzigou, V. Zhukov, S. Mondy, G. Abu el Heba, V. Cosson, T. H. N. Ellis, M. Ambrose, J. Wen, M. Tadege, I. Tikhonovich, K. S. Mysore, J. Putterill, J. Hofer, A. Y. Borisov, P. Ratet, NODULE ROOT and COCHLEATA maintain nodule development and are Legume orthologs of Arabidopsis BLADE-ON-PETIOLE genes. *Plant Cell* 24, 4498–4510 (2012).
- S. Su, Y. Lei, X. Zhou, T. Suzuki, W. Xiao, T. Higashiyama, A BLADE-ON-PETIOLE orthologue regulates corolla differentiation in the proximal region in Torenia fournieri. *Nat. Commun.* 14, 4763 (2023).
- J. L. Yaxley, W. Jablonski, J. B. Reid, Leaf and flower development in pea (Pisum sativum L.): Mutants cochleata and unifoliata. *Ann. Bot.* 88, 225–234 (2001).
- J. C. Preston, L. C. Hileman, Developmental genetics of floral symmetry evolution. *Trends Plant Sci.* 14, 147–154 (2009).
- T. S. Dunivant, V. Singh, K. E. Livingston, J. D. Ross, L. C. Hileman, CYCLOIDEA paralogs function partially redundantly to specify dorsal flower development in *Mimulus lewisii*. *Am. J. Bot.* 111, e16271 (2024).
- D. J. Gingerich, J. M. Gagne, D. W. Salter, H. Hellmann, M. Estelle, L. Ma, R. D. Vierstra, Cullins 3a and 3b assemble with members of the broad complex/tramtrack/bric-a-brac (BTB) protein family to form essential ubiquitin-protein ligases (E3s) in Arabidopsis. *J. Biol. Chem.* 280, 18810–18821 (2005).
- R. Geyer, S. Wee, S. Anderson, J. Yates, D. A. Wolf, BTB/POZ domain proteins are putative substrate adaptors for cullin 3 ubiquitin ligases. Mol. Cell 12, 783–790 (2003).
- B. Zhang, M. Holmlund, S. Lorrain, M. Norberg, L. Bako, C. Fankhauser, O. Nilsson, BLADE-ON-PETIOLE proteins act in an E3 ubiquitin ligase complex to regulate PHYTOCHROME INTERACTING FACTOR 4 abundance. eLife 6, e26759 (2017).
- H. Chahtane, B. Zhang, M. Norberg, M. LeMasson, E. Thevenon, L. Bako, R. Benlloch, M. Holmlund, F. Parcy, O. Nilsson, G. Vachon, LEAFY activity is post-transcriptionally regulated by BLADE ON PETIOLE2 and CULLIN3 in Arabidopsis. *New Phytol.* 220, 579–592 (2018).

SCIENCE ADVANCES | RESEARCH ARTICLE

- S. Tahtiharju, A. S. Rijpkema, A. Vetterli, V. A. Albert, T. H. Teeri, P. Elomaa, Evolution and diversification of the CYC/TB1 gene family in Asteraceae—A comparative study in Gerbera (Mutisieae) and sunflower (Heliantheae). Mol. Biol. Evol. 29, 1155–1166 (2012).
- X. Yang, H.-B. Pang, B.-L. Liu, Z.-J. Qiu, Q. Gao, L. Wei, Y. Dong, Y.-Z. Wang, Evolution of double positive autoregulatory feedback loops in CYCLOIDEA2 clade genes is associated with the origin of floral zygomorphy. *Plant Cell* 24, 1834–1847 (2012).
- P. Cubas, E. Coen, J. M. Zapater, Ancient asymmetries in the evolution of flowers. Curr. Biol. 11, 1050–1052 (2001).
- A. Busch, S. Zachgo, Control of corolla monosymmetry in the Brassicaceae Iberis amara. Proc. Natl. Acad. Sci. U.S.A. 104, 16714–16719 (2007).
- X. Yang, Y. Wang, T.-X. Liu, Q. Liu, J. Liu, T.-F. Lü, R.-X. Yang, F.-X. Guo, Y.-Z. Wang, CYCLOIDEA-like genes control floral symmetry, floral orientation, and nectar guide patterning. *Plant Cell* 35, 2799–2820 (2023).
- V. L. Bergbusch, A note on the manipulation of flower symmetry in Antirrhinum majus. Ann. Bot. 83, 483–488 (1999).
- J. H. Jun, C. M. Ha, J. C. Fletcher, BLADE-ON-PETIOLE1 coordinates organ determinacy and axial polarity in Arabidopsis by directly activating ASYMMETRIC LEAVES2. Plant Cell 22, 62–76 (2010).
- 48. C. Kuhlemeier, M. C. P. Timmermans, The Sussex signal: Insights into leaf dorsiventrality. Development 143, 3230–3237 (2016).
- J. I. Clark, E. S. Coen, The cycloidea gene can respond to a common dorsoventral prepattern in Antirrhinum. *Plant J.* 30, 639–648 (2002).
- Y.-W. Yuan, J. M. Sagawa, R. C. Young, B. J. Christensen, H. D. Bradshaw, Genetic dissection of a major anthocyanin QTL contributing to pollinator-mediated reproductive isolation between sister species of Mimulus. *Genetics* 194, 255–263 (2013).
- C. Owen, H. D. Bradshaw, Induced mutations affecting pollinator choice in *Mimulus lewisii* (Phrymaceae). *Arthropod. Plant Interact.* 5, 235–244 (2011).
- A. M. LaFountain, W. Chen, W. Sun, S. Chen, H. A. Frank, B. Ding, Y.-W. Yuan, Molecular basis of overdominance at a flower color locus. G3 (Bethesda) 7, 3947–3954 (2017).
- Y.-W. Yuan, J. M. Sagawa, V. S. Di Stilio, H. D. Bradshaw, Bulk segregant analysis of an induced floral mutant identifies a MIXTA-like R2R3 MYB controlling nectar guide formation in *Mimulus lewisii*. Genetics 194, 523–528 (2013).
- J. M. Sagawa, L. E. Stanley, A. M. LaFountain, H. A. Frank, C. Liu, Y.-W. Yuan, An R2R3-MYB transcription factor regulates carotenoid pigmentation in *Mimulus lewisii* flowers. *New Phytol.* 209, 1049–1057 (2016).
- B. Ding, F. Mou, W. Sun, S. Chen, F. Peng, H. D. Bradshaw, Y.-W. Yuan, A dominant-negative actin mutation alters corolla tube width and pollinator visitation in *Mimulus lewisii*. New Phytol. 213, 1936–1944 (2016).
- L. E. Stanley, B. Ding, W. Sun, F. Mou, C. Hill, S. Chen, Y.-W. Yuan, A tetratricopeptide repeat protein regulates carotenoid biosynthesis and chromoplast development in monkeyflowers (Mimulus). *Plant Cell* 32, 1536–1555 (2020).
- K.W. Earley, J. R. Haag, O. Pontes, K. Opper, T. Juehne, K. Song, C. S. Pikaard, Gatewaycompatible vectors for plant functional genomics and proteomics. *Plant J.* 45, 616–629 (2006).
- X. Ma, Q. Zhang, Q. Zhu, W. Liu, Y. Chen, R. Qiu, B. Wang, Z. Yang, H. Li, Y. Lin, Y. Xie, R. Shen, S. Chen, Z. Wang, Y. Chen, J. Guo, L. Chen, X. Zhao, Z. Dong, Y. G. Liu, A robust CRISPR/Cas9 system for convenient, high-efficiency multiplex genome editing in monocot and dicot plants. *Mol. Plant* 8, 1274–1284 (2015).
- E. M. Kramer, Methods for studying the evolution of plant reproductive structures:
 Comparative gene expression techniques. Methods Enzymol. 395, 617–636 (2005).
- R. Waadt, L. K. Schmidt, M. Lohse, K. Hashimoto, R. Bock, J. Kudla, Multicolor bimolecular fluorescence complementation reveals simultaneous formation of alternative CBL/CIPK complexes in planta. *Plant J.* 56, 505–516 (2008).

- 61. B. Ding, Y.-W. Yuan, Testing the utility of fluorescent proteins in *Mimulus lewisii* by an *Agrobacterium*-mediated transient assay. *Plant Cell Rep.* **35**, 771–777 (2016).
- O. Levin-Kravets, N. Tanner, N. Shohat, I. Attali, T. Keren-Kaplan, A. Shusterman, S. Artzi, A. Varvak, Y. Reshef, X. Shi, O. Zucker, T. Baram, C. Katina, I. Pilzer, S. Ben-Aroya, G. Prag, A bacterial genetic selection system for ubiquitylation cascade discovery. *Nat. Methods* 13, 945–952 (2016).
- 63. R. Zavaliev, R. Mohan, T. Chen, X. Dong, Formation of NPR1 condensates promotes cell survival during the plant immune response. *Cell* **182**, 1093–1108.e18 (2020).
- A. Larsson, AliView: A fast and lightweight alignment viewer and editor for large datasets. Bioinformatics 30, 3276–3278 (2014).
- K. Tamura, G. Stecher, S. Kumar, MEGA11: Molecular evolutionary genetics analysis version 11. Mol. Biol. Evol. 38, 3022–3027 (2021).
- R. P. Hellens, A. C. Allan, E. N. Friel, K. Bolitho, K. Grafton, M. D. Templeton,
 Karunairetnam, A. P. Gleave, W. A. Laing, Transient expression vectors for functional genomics, quantification of promoter activity and RNA silencing in plants. *Plant Methods* 1. 13 (2005).
- C. Coutu, J. Brandle, D. Brown, K. Brown, B. Miki, J. Simmonds, D. D. Hegedus, pORE: A modular binary vector series suited for both monocot and dicot plant transformation. *Transgenic Res.* 16, 771–781 (2007).
- B. Ding, R. Xia, Q. Lin, V. Gurung, J. M. Sagawa, L. E. Stanley, M. Strobel, P. K. Diggle,
 B. C. Meyers, Y.-W. Yuan, Developmental genetics of corolla tube formation: Role of the tasiRNA-ARF pathway and a conceptual model. *Plant Cell* 32, 3452–3468 (2020).

Acknowledgments: We thank C. Morse, M. Opel, and M. Moriarty for extraordinary plant care in the UConn EEB Research Greenhouses. We are grateful to Y. Ma (Central Laboratory of the College of Horticulture, Nanjing Agricultural University) for assistance in using the highresolution confocal laser microscope (ZEISS, LSM800). The plasmids pACYC-RC3, pCDF-Ub, and pETDuet-1: Flag-WRKY70+GST, were provided by X. Dong from Duke University. The cDNA of D. anthriscifolium was a gift from R. Zhang from Northwest A&F University. E. Kramer at Harvard University provided laboratory space for B.D. to learn in situ hybridization techniques. W. Fan and Y. Zhou helped with the drawing art. This project was supported by the Bioinformatics Center of Nanjing Agricultural University. Funding: This work was financially supported by grants from the National Natural Science Foundation of China to B.D. (32122078) and F.C. (32230098), the Fundamental Research Funds for the Central Universities (YDZX2023018), and Nanjing Agricultural University start-up funds to B.D. and NSF grants (IOS-1755373 and IOS-1827645) to Y.-W.Y. Author contributions: Conceptualization: B.D., Y.G., and Y.-W.Y. Investigation: Y.G., J.L., and J.H. Visualization: J.H., J.L., and B.D. Resources: B.D., J.L., and Y.-W.Y. Formal analysis: Y.G., B.D., J.L., and J.H. Validation: Y.G., B.D., J.L., J.H., Y.Y., Z.G., Z.Q., Y.Z., Y.K., Q.L., L.Y., and J.W. Writing—original draft: Y.G., Y.-W.Y., and B.D. Writing—review and editing: Y.G., and B.D. Supervision: B.D., Y.-W.Y., S.C., and F.C. Funding acquisition: B.D., Y.-W.Y., and F.C. Project administration: B.D., Y.G., and Y.-W.Y. Competing interests: The authors declare that they have no competing interests. Data and materials availability: All data needed to evaluate the conclusions in the paper are present in the paper and/or the Supplementary Materials. Genome sequence data have been deposited in the NCBI Sequence Read Archive (SRR26855520). The plasmids can be provided by B.D. pending scientific review and a completed material transfer agreement. Requests for the plasmids should be submitted to: B.D.

Submitted 2 February 2024 Accepted 8 July 2024 Published 14 August 2024 10.1126/sciadv.ado4571